

# Suppression of GFAP toxicity by $\alpha$ B-crystallin in mouse models of Alexander disease

Tracy L. Hagemann<sup>1,\*</sup>, Wilbert C. Boelens<sup>3</sup>, Eric F. Wawrousek<sup>4</sup> and Albee Messing<sup>1,2</sup>

<sup>1</sup>Waisman Center and <sup>2</sup>Department of Comparative Biosciences, University of Wisconsin, Madison, WI 53705, USA, <sup>3</sup>Department of Biomolecular Chemistry 271, Nijmegen Center for Molecular Life Sciences, Radboud University, PO Box 9101, NL-6500 HB Nijmegen, The Netherlands and <sup>4</sup>National Eye Institute, National Institutes of Health, DHHS, Bethesda, MD 20892, USA

Received December 10, 2008; Revised December 30, 2008; Accepted January 5, 2009

**Alexander disease (AxD) is a primary disorder of astrocytes caused by dominant mutations in the gene for glial fibrillary acidic protein (GFAP). These mutations lead to protein aggregation and formation of Rosenthal fibers, complex astrocytic inclusions that contain GFAP, vimentin, plectin, ubiquitin, Hsp27 and  $\alpha$ B-crystallin. The small heat shock protein  $\alpha$ B-crystallin (Cryab) regulates GFAP assembly, and elevation of Cryab is a consistent feature of AxD; however, its role in Rosenthal fibers and AxD pathology is not known. Here, we show in AxD mouse models that loss of Cryab results in increased mortality, whereas elevation of Cryab rescues animals from terminal seizures. When mice with Rosenthal fibers induced by over-expression of GFAP are crossed into a Cryab-null background, over half die at 1 month of age. Restoration of Cryab expression through the GFAP promoter reverses this outcome, showing the effect is astrocyte-specific. Conversely, in mice engineered to express both AxD-associated mutations and elevated GFAP, which despite natural induction of Cryab also die at 1 month, transgenic over-expression of Cryab results in a markedly reduced CNS stress response, restores expression of the glutamate transporter Glt1 (EAAT2) and protects these animals from death. In its most common form, AxD is a devastating neurodegenerative disease, with early onset, characterized by seizures, spasticity and developmental delays, ultimately leading to death. Cryab plays a critical role in tempering AxD pathology and should be investigated as a therapeutic target for this and other diseases with astropathology.**

## INTRODUCTION

Alexander disease (AxD) is a rare and typically fatal neurodegenerative disorder of childhood caused by mutations in the astrocyte-specific intermediate filament glial fibrillary acidic protein (GFAP) (1,2). Common initial symptoms include seizures and spasticity, which in the early onset form, progress to death within 3–4 years. Although AxD usually manifests during infancy, GFAP mutations are also responsible for less severe cases with juvenile or adult onset (3), but no specific genotype–phenotype relationships have yet been identified. Three obvious hot spots for mutations exist, with approximately half of all patients affected at R79, R239 or R416, but many other mutations are distributed throughout the rod and tail domains of the protein (3). In some cases, the same

mutation (i.e. R416W) is associated with all three forms of the disease.

The consistent pathological hallmark of AxD is the formation of cytoplasmic protein aggregates within astrocytes known as Rosenthal fibers. In addition to GFAP, these aggregates contain many other components, including vimentin, the cytoskeletal crosslinker plectin (4), ubiquitin and the small stress proteins Hsp25 and  $\alpha$ B-crystallin (5,6). As with other protein aggregation disorders of the central nervous system (7), the question of whether the Rosenthal fibers are toxic or protective has not yet been resolved.

Although the genetic basis for AxD is now firmly established, little is known regarding the mechanisms by which GFAP mutations lead to disease (8,9). Using mouse models, we have shown that Rosenthal fibers can originate from either expression

\*To whom correspondence should be addressed at: Waisman Center 715, University of Wisconsin, 1500 Highland Avenue, Madison, WI 53705, USA. Tel: +1 6082639192; Fax: +1 6082634364; Email: hagemann@waisman.wisc.edu

of mutant protein or over-expression of wild-type protein, and that elevation in total levels of GFAP may be a critical element in pathogenesis (10–12). GFAP mutations are dominant, generating protein with a toxic gain of function, but etiologically it is also possible that astrocyte dysfunction occurs in part due to depletion and consequent loss of function in other cellular elements, such as  $\alpha$ B-crystallin (Cryab). Rosenthal fibers are associated with shifts in the equilibrium of both GFAP and Cryab from the soluble to insoluble protein pool (6,13).

Cryab was first identified in the lens, but is now viewed as part of a multi-gene family of widely expressed small heat shock proteins in which Cryab has been given the designation Hspb5 (14). Functionally, Cryab acts as a chaperone (15–17) and is normally expressed in several tissues outside of the eye even in the absence of stress (18,19). Cryab associates with intermediate filaments, especially type III filaments such as vimentin (20), desmin (21) and GFAP (22), where it regulates assembly and assists intermediate filaments in recovery from stress by preventing untimely filament–filament interactions that would otherwise lead to aggregation. Recently, Ghosh *et al.* (23) identified six distinct regions within human CRYAB that are preferential binding sites for human GFAP.

Cryab also negatively regulates apoptosis through multiple mechanisms (24–26), maintains redox homeostasis (27) and binds to the 20S proteasome, where it may facilitate degradation of misfolded proteins (28,29). In the absence of Cryab, knockout mice show normal lens development and age-related degeneration of skeletal muscle, but otherwise have no overt phenotype. A recent study, however, show Cryab<sup>-/-</sup> mice to be more susceptible to experimental autoimmune encephalomyelitis (EAE) with an increase in inflammation and glial apoptosis (30).

Although Cryab is normally expressed at low levels in the brain, its induction in several neurodegenerative diseases, abundance in Rosenthal fibers and apparent role in regulating interactions of intermediate filament subunits led us to consider whether it could play an active role in the pathogenesis of AxD. Studies have shown that increased levels of Cryab solubilize GFAP and decrease aggregation *in vitro* (20,22,31). By genetically manipulating levels of Cryab in mouse models of AxD, we find that deficiency of Cryab exacerbates the AxD phenotype, causing death in lines that are normally viable. In contrast, enhancing Cryab beyond naturally occurring levels rescues AxD mice from the otherwise lethal effects of GFAP mutation and excess.

## RESULTS

### Loss of Cryab in GFAP transgenic mice decreases survival

To determine the impact of Cryab on Rosenthal fiber formation and AxD pathology, we crossed transgenic mice expressing wild-type human GFAP (line Tg73.7 (10), hereafter referred to as GFAP<sup>Tg</sup>) with Cryab<sup>-/-</sup> knockout mice. The resulting GFAP<sup>Tg</sup>;Cryab<sup>-/-</sup> animals still form ubiquitinated astrocytic protein aggregates (Fig. 1A and B), which under electron microscopy consist of electron dense osmiophilic structures surrounded by swirls of intermediate filaments, consistent with Rosenthal fibers (32) (Fig. 1C). Typically, GFAP<sup>Tg</sup> mice have <10% mortality at ~30 days of age, whereas in the context of

Cryab deficiency, two-thirds of Cryab<sup>-/-</sup> animals and one-third of Cryab<sup>+/-</sup> animals die at a median age of 32 days (Fig. 1D). Although our results show that Cryab is not necessary for Rosenthal fiber formation, the increased number of mice showing lethality at this age clearly demonstrates the importance of Cryab in maintaining viability for the GFAP<sup>Tg</sup> model. In contrast to GFAP<sup>Tg</sup> mice, heterozygous GFAP<sup>+R236H</sup> knock-in animals with an AxD-associated mutation (equivalent to R239H in human GFAP) remain viable in the Cryab<sup>-/-</sup> background.

### Transgenic expression of Cryab in astrocytes restores survival proportions for GFAP<sup>Tg</sup> mice

To determine whether lethality in the GFAP<sup>Tg</sup>;Cryab<sup>-/-</sup> animals is a result of the loss of Cryab in astrocytes, we generated transgenic mice with the *Cryab* gene under the control of the human *GFAP* promoter to target expression to astrocytes (Fig. 2A). Several transgenic lines with varying levels of expression were produced (Fig. 2B). The highest expressing line (Tg141.6) was used in subsequent crosses and experiments (hereafter referred to as Cryab<sup>Tg</sup>).

Mice were bred to combine both GFAP<sup>Tg</sup> and Cryab<sup>Tg</sup> in the Cryab<sup>-/-</sup> background. The majority of GFAP<sup>Tg</sup>;Cryab<sup>-/-</sup> animals died at ~30 days of age; however, almost all of the mice with the added Cryab transgene survived to a minimum of 3 months (Fig. 2C). These animals had increased body weight compared with GFAP<sup>Tg</sup> littermates (Supplementary Material, Fig. S1). Rosenthal fibers were apparent in the GFAP<sup>Tg</sup>;Cryab<sup>-/-</sup>; Cryab<sup>Tg</sup> mice with both light and electron microscopy (Fig. 2D and E). As expected, Cryab<sup>-/-</sup> mice show astrocyte-specific expression of the Cryab transgene under the control of the GFAP promoter (Fig. 2F–M). Survival of the Cryab<sup>Tg</sup> animals in the null background confirms that lethality in the GFAP<sup>Tg</sup> animals is not due to the loss of Cryab in neurons, and that the protective effects of Cryab are astrocyte-specific.

### Elevated Cryab rescues GFAP<sup>Tg</sup>;GFAP<sup>+R236H</sup> mice from lethal seizures and reduces Rosenthal fibers and GFAP in hippocampus

Given the results of previous studies showing the dissolution of GFAP filaments or aggregates by Cryab *in vitro* (20,22,31), and the increase in body weight observed in the GFAP<sup>Tg</sup>;Cryab<sup>Tg</sup> mice (Supplementary Material, Fig. S1), we hypothesized that increased expression of the heat shock protein may solubilize or disaggregate Rosenthal fibers *in vivo* and have a beneficial effect on the AxD phenotype. Since both GFAP<sup>Tg</sup> and GFAP<sup>+R236H</sup> animals have a relatively mild phenotype, we sought a more severe model in which to test for potential rescue by Cryab. Previously, we found that crossing GFAP<sup>+R236H</sup> knock-in to GFAP<sup>Tg</sup> transgenic mice creates GFAP<sup>Tg</sup>;GFAP<sup>+R236H</sup> double-positive offspring that consistently die at ~30 days of age (12). Such GFAP<sup>Tg</sup>;GFAP<sup>+R236H</sup> animals display a synergistic increase in insoluble GFAP, doubling that observed in GFAP<sup>Tg</sup> mice, and observation showed severe spontaneous seizures immediately before death (12). However, when we crossed GFAP<sup>Tg</sup> and GFAP<sup>+R236H</sup> with Cryab<sup>Tg</sup> to create triple-positive mice, all of the mice inheriting Cryab<sup>Tg</sup> survived, whereas those carrying GFAP<sup>Tg</sup> and GFAP<sup>+R236H</sup> combined without Cryab<sup>Tg</sup> died (Fig. 3A).

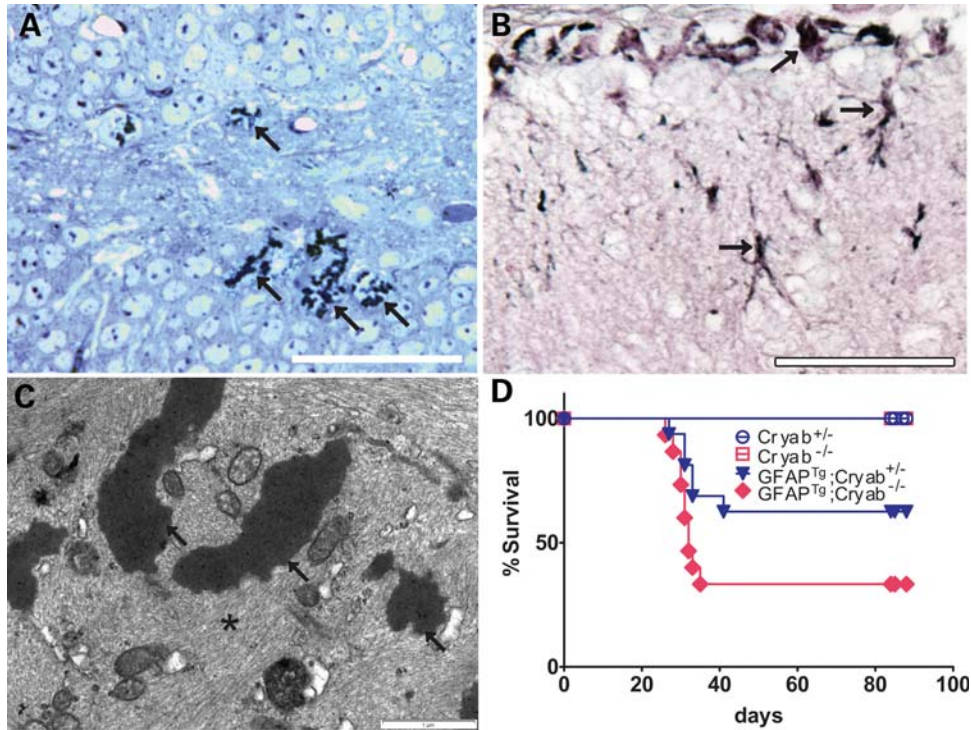


**Figure 1.** GFAP transgenic mice form Rosenthal fibers without Cryab, but show increased mortality. (A) Toluidine Blue staining in the hippocampal dentate gyrus reveals clusters of Rosenthal fiber aggregates (arrows) in a GFAP<sup>Tg</sup>;Cryab<sup>-/-</sup> mouse at 3 months of age (50 μm scale bar). (B) Immunohistochemistry demonstrates ubiquitination of Rosenthal fibers (gray/blue, indicated with arrows) near the pial surface of the superior colliculus (P25, 50 μm scale bar). (C) Ultrastructurally, electron microscopy shows dense osmiophilic structures (arrows) surrounded by swirls (asterisk) of intermediate filaments (3 months of age, 1 μm scale bar). (D) Survival proportions show a significant difference ( $P \leq 0.0001$ , log-rank Mantel-Cox test) and indicate a dose response for Cryab in GFAP<sup>Tg</sup> mice, with Cryab<sup>+/-</sup> and Cryab<sup>-/-</sup> exhibiting 63 and 33% survival, respectively (Cryab<sup>+/-</sup>  $n = 19$ , Cryab<sup>-/-</sup>  $n = 11$ , GFAP<sup>Tg</sup>;Cryab<sup>+/-</sup>  $n = 16$ , GFAP<sup>Tg</sup>;Cryab<sup>-/-</sup>  $n = 15$ ).

Fewer Rosenthal fibers were apparent in GFAP<sup>Tg</sup>;GFAP<sup>+/-</sup><sub>R236H</sub>;Cryab<sup>Tg</sup> hippocampi compared with GFAP<sup>Tg</sup>;GFAP<sup>+/-</sup><sub>R236H</sub> mice (Fig. 3B and C). To quantify this effect, we analyzed GFAP levels in soluble versus insoluble protein fractions (see Materials and Methods). Increased Cryab expression significantly reduced (35%) both soluble and insoluble GFAP levels in GFAP<sup>Tg</sup>;GFAP<sup>+/-</sup><sub>R236H</sub>;Cryab<sup>Tg</sup> compared with GFAP<sup>Tg</sup>;GFAP<sup>+/-</sup><sub>R236H</sub> mice (Fig. 3D). GFAP<sup>Tg</sup>;Cryab<sup>Tg</sup> mice also showed a reduction in the insoluble fraction of GFAP; however, there were no significant changes in solubility in GFAP<sup>+/-</sup><sub>R236H</sub>;Cryab<sup>Tg</sup> mice (Fig. 3D). Increased Cryab may be able to compensate for the high levels of wild-type GFAP in the GFAP<sup>Tg</sup> mice, whereas the mutant forms of GFAP are likely more resistant to dissolution (13).

#### Cryab<sup>Tg</sup> reduces the stress response and restores Glt1 expression in GFAP<sup>Tg</sup>;GFAP<sup>+/-</sup><sub>R236H</sub> mice

The transcription factor Nrf2 (Nfe212) regulates the expression of phase II detoxification genes including peroxiredoxins, oxidoreductases such as Nqo1, and genes involved in the glutathione and thioredoxin systems through the anti-oxidant response element (ARE). We showed previously that GFAP<sup>Tg</sup> and GFAP<sup>+/-</sup><sub>R236H</sub> mice each have dramatic increases in ARE-induced activity and a corresponding elevation of Nrf2-regulated gene transcripts (11,12). GFAP<sup>Tg</sup>;GFAP<sup>+/-</sup><sub>R236H</sub> mice demonstrate over a 5-fold increase in the expression

of both Nrf2 and its target gene Nqo1 (Fig. 4A and B). The addition of the Cryab transgene reduced both Nrf2 and Nqo1 transcript levels by >60%, and to near that of wild-type in the GFAP<sup>+/-</sup><sub>R236H</sub> and GFAP<sup>Tg</sup> mice separately.

We have recently shown that adult GFAP<sup>+/-</sup><sub>R236H</sub> mice have reduced levels of the glutamate transporter Glt1 (Slc1a2, EAAT2; R. Tian, X. Wu, T.L. Hagemann, A.A. Sosunov, Z. Su, T.F. Franke, P.B. Fisher, A. Messing, G.M. McKhann, J.E. Goldman, in preparation) and are more susceptible to kainate-induced seizures (12). Since astrocytes are responsible for regulating synaptic glutamate uptake primarily through Glt1, and seizures can be induced by elevated glutamate and excitotoxicity (33), we measured hippocampal Glt1 expression in GFAP<sup>Tg</sup>;GFAP<sup>+/-</sup><sub>R236H</sub> mice. These animals show a 70% reduction in Glt1 expression (Fig. 4C), whereas GFAP<sup>Tg</sup>;GFAP<sup>+/-</sup><sub>R236H</sub>;Cryab<sup>Tg</sup> animals show nearly a 2-fold increase in Glt1 transcripts ( $P = 0.0182$ ). Glt1 protein shows a similar pattern with restoration of expression to near that of wild-type (Fig. 4D), demonstrating a potential mechanism for the rescue effect and increased survival.

#### Elevated Cryab reduces GFAP accumulation in GFAP<sup>Tg</sup> mice and reduces the stress response in both GFAP transgenic and mutant mice

To further detail the role of Cryab in AxD pathology in older animals, we analyzed Rosenthal fiber distribution and the

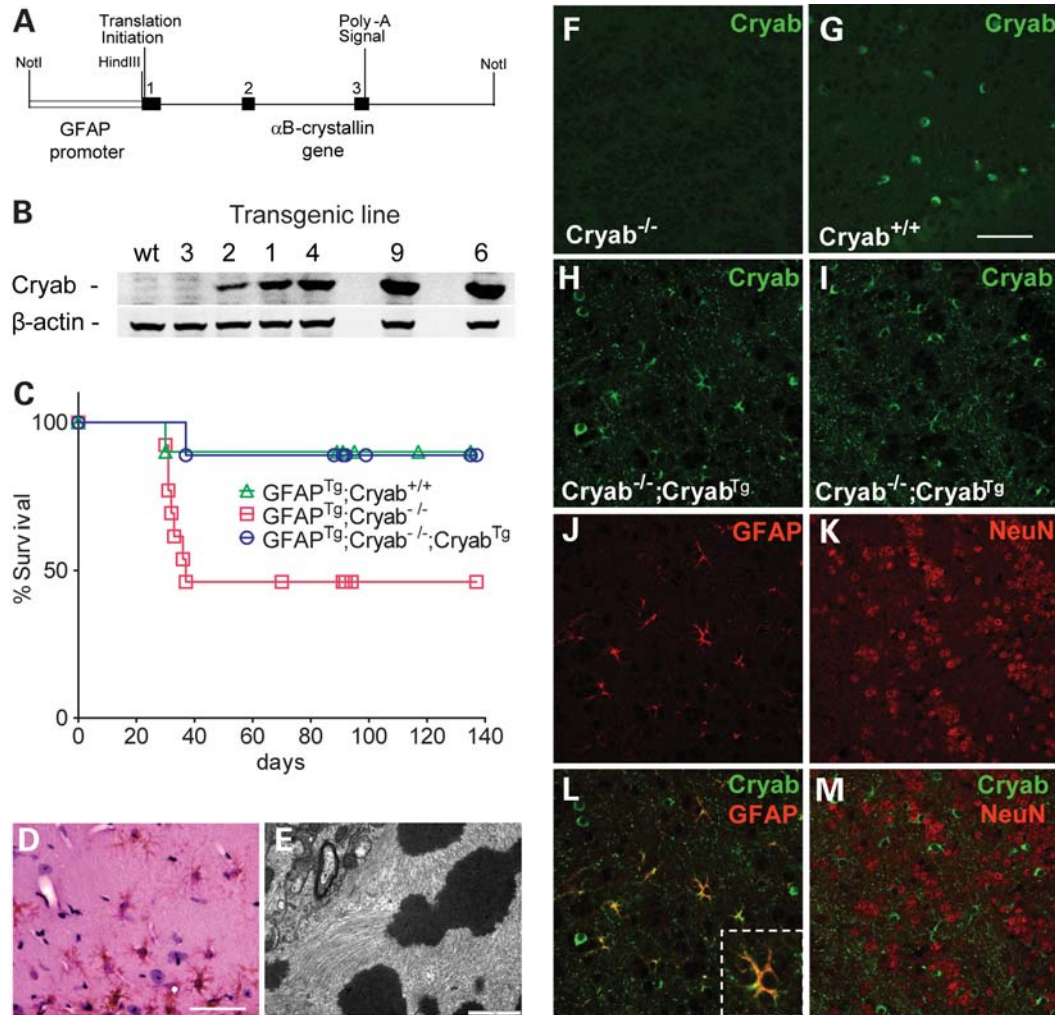


**Figure 2.** Rescue of lethal phenotype in  $\text{GFAP}^{\text{Tg}};\text{Cryab}^{-/-}$  mice by astrocyte-specific restoration of  $\text{Cryab}$  expression. (A) The Tg141 transgene, consisting of the human GFAP promoter ligated to the hamster  $\text{Cryab}$  gene, was constructed to over-express  $\text{Cryab}$  in astrocytes. (B) Several founder lines were generated (Tg141 1–4, 6, 9) with varying levels of  $\text{Cryab}$  expression, as shown by western analysis. (C) Survival proportions show lethality in 54% of  $\text{GFAP}^{\text{Tg}};\text{Cryab}^{-/-}$  mice ( $n = 13$ ) compared with  $\sim 10\%$  of  $\text{GFAP}^{\text{Tg}};\text{Cryab}^{-/-};\text{Cryab}^{\text{Tg}}$  ( $n = 9$ ) and  $\text{GFAP}^{\text{Tg}};\text{Cryab}^{+/+}$  ( $n = 10$ ) littermates ( $P = 0.0281$ , log-rank Mantel–Cox test). (D) Rosenthal fibers under light microscopy are eosinophilic (red) and appear to outline astrocytic processes in the  $\text{GFAP}^{\text{Tg}};\text{Cryab}^{-/-};\text{Cryab}^{\text{Tg}}$  mice (50  $\mu\text{m}$  scale bar). (E) Fibers in  $\text{GFAP}^{\text{Tg}};\text{Cryab}^{-/-};\text{Cryab}^{\text{Tg}}$  mice have the same ultrastructural qualities as those in  $\text{GFAP}^{\text{Tg}}$  mice (1  $\mu\text{m}$  scale bar). (F, G) Immunofluorescence shows the absence of  $\text{Cryab}$  in null mice (F) compared with wild-type (G, 50  $\mu\text{m}$  scale bar) with confocal microscopy using equivalent gain. (H, J, L) Expression of the  $\text{Cryab}^{\text{Tg}}$  (green) in  $\text{Cryab}^{-/-}$  animals is astrocyte-specific (GFAP, red). (L) The inset shows an enlarged view of an astrocyte from the same field expressing  $\text{Cryab}$  (yellow). (I, K, M) No  $\text{Cryab}$  (green) staining is apparent in neurons (NeuN, red). (F–M) Olfactory bulb (granular layer) shown at same magnification.

cellular stress response in the  $\text{GFAP}^{\text{Tg}}$  and  $\text{GFAP}^{+/R236H}$  models separately. In brains from the  $\text{GFAP}^{\text{Tg}};\text{Cryab}^{\text{Tg}}$  animals, Rosenthal fibers appeared more diffuse (Fig. 5A and B), with differences in anatomical distribution (Supplementary Material, Table S1). However, electron microscopy demonstrated the same ultrastructure for aggregates in both single  $\text{GFAP}^{\text{Tg}}$  and double  $\text{GFAP}^{\text{Tg}};\text{Cryab}^{\text{Tg}}$  positive astrocytes (Fig. 5C and D). Heterozygous  $\text{GFAP}^{+/R236H}$  mice showed no obvious differences in Rosenthal fiber distribution when crossed with the  $\text{Cryab}^{\text{Tg}}$  line, correlating with the lack of effect on GFAP solubility.

To characterize and quantify the effect of increased  $\text{Cryab}$  expression on the stress response in AxD mice, a reporter transgene for Nrf2 activation was introduced consisting of the ARE driving the human placental alkaline phosphatase

(hPAP) gene. With increased  $\text{Cryab}$  expression, the stress response is significantly decreased by almost 90% in both  $\text{GFAP}^{\text{Tg}}$  and  $\text{GFAP}^{+/R236H}$  mice at 6 weeks of age (Fig. 5E). Histological staining for the alkaline phosphatase reporter shows reduced activity in most regions including cortex, subpial regions, corpus callosum, midbrain, cerebellum, olfactory bulb and hippocampus (Fig. 5F–I).

## DISCUSSION

The small heat shock protein  $\alpha\text{B}$ -crystallin is a multi-tasking chaperone with important roles in cytoskeletal assembly, protein turnover, redox homeostasis and apoptosis.  $\text{Cryab}$  provides chaperone functions for cytoskeletal and other proteins

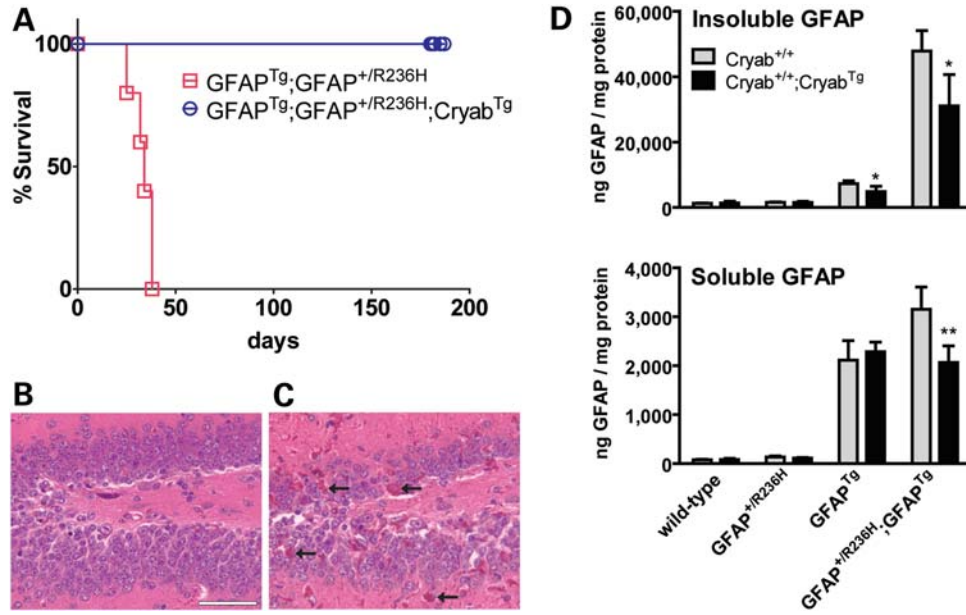


**Figure 3.** Increased Cryab expression rescues lethal seizures and reduces GFAP levels and Rosenthal fibers in  $GFAP^{Tg};GFAP^{+/R236H}$  mice. (A) Hundred percent of  $GFAP^{Tg};GFAP^{+/R236H}$  mice die at an early age [ $\sim 30$  days (12); for littermates shown ( $n = 5$ ), median age of death = 34] compared with 100% survival in  $GFAP^{Tg};GFAP^{+/R236H}$  mice expressing Cryab<sup>Tg</sup> ( $n = 8$ ;  $P = 0.0002$ , log-rank Mantel–Cox test). (B, C) Fewer Rosenthal fibers (red) appear in the hippocampus of  $GFAP^{Tg};GFAP^{+/R236H};Cryab^{Tg}$  (B, 50  $\mu m$  scale bar) compared with  $GFAP^{Tg};GFAP^{+/R236H}$  mice (C, arrows show representative Rosenthal fibers). (D) GFAP levels in the different transgenic and mutant mice comparing those with or without the Cryab<sup>Tg</sup> (P26) show that elevated Cryab decreases insoluble GFAP in hippocampi from  $GFAP^{Tg}$  mice ( $*P = 0.0409$ ) and decreases both the soluble ( $**P = 0.0088$ ) and insoluble ( $*P = 0.0259$ ) pool of GFAP in  $GFAP^{+/R236H}$  animals. Cryab<sup>Tg</sup> does not significantly affect GFAP expression or solubility in wild-type or  $GFAP^{+/R236H}$  mice.

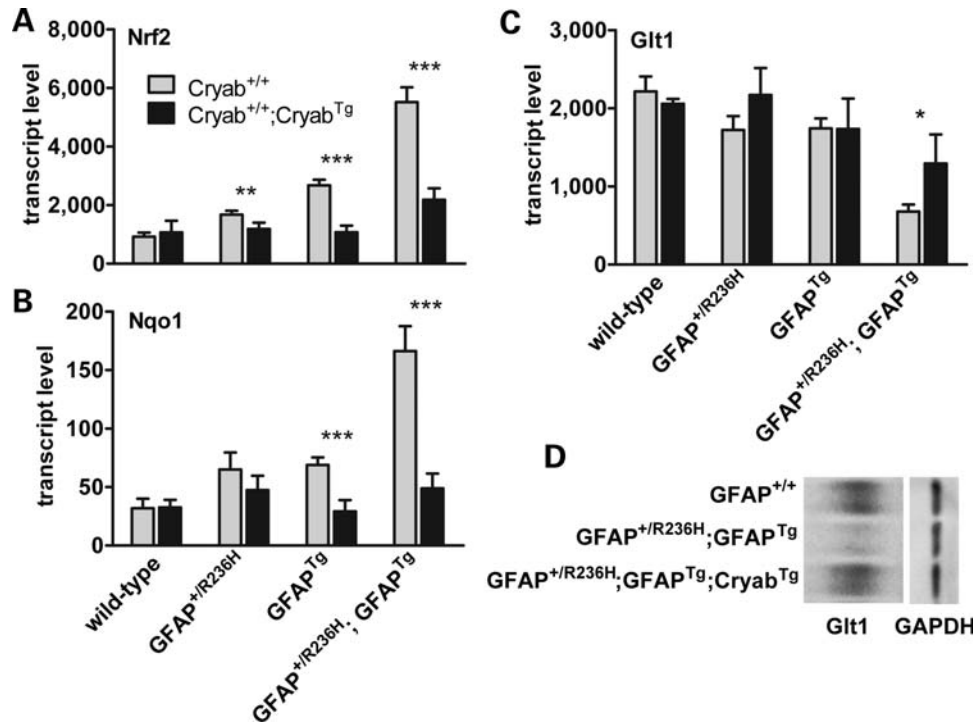


**Figure 4.** Cryab<sup>Tg</sup> decreases the stress response and restores Glt1 expression in  $GFAP^{Tg};GFAP^{+/R236H}$  hippocampus. (A, B) Quantitative PCR shows reduced expression of stress genes Nrf2 (A,  $**P = 0.0079$ ,  $***P < 0.0001$ ) and Nqo1 (B,  $***P = 0.0005$  for  $GFAP^{Tg}$ ,  $***P < 0.0001$  for  $GFAP^{Tg};GFAP^{+/R236H}$ ) with increased expression of Cryab and (C) increased expression of the glutamate transporter Glt1 ( $*P = 0.0182$ ). Unpaired *t*-tests (two-tailed) were used to generate *P*-values for comparisons. Error bars represent standard deviation. (D) Western analysis of Glt1 protein in hippocampi from  $GFAP^{Tg};GFAP^{+/R236H}$  and  $GFAP^{Tg};GFAP^{+/R236H};Cryab^{Tg}$  mice shows the same pattern as Glt1 transcription with Cryab<sup>Tg</sup> restoring expression close to that of wild-type mice. GAPDH expression is shown for control.

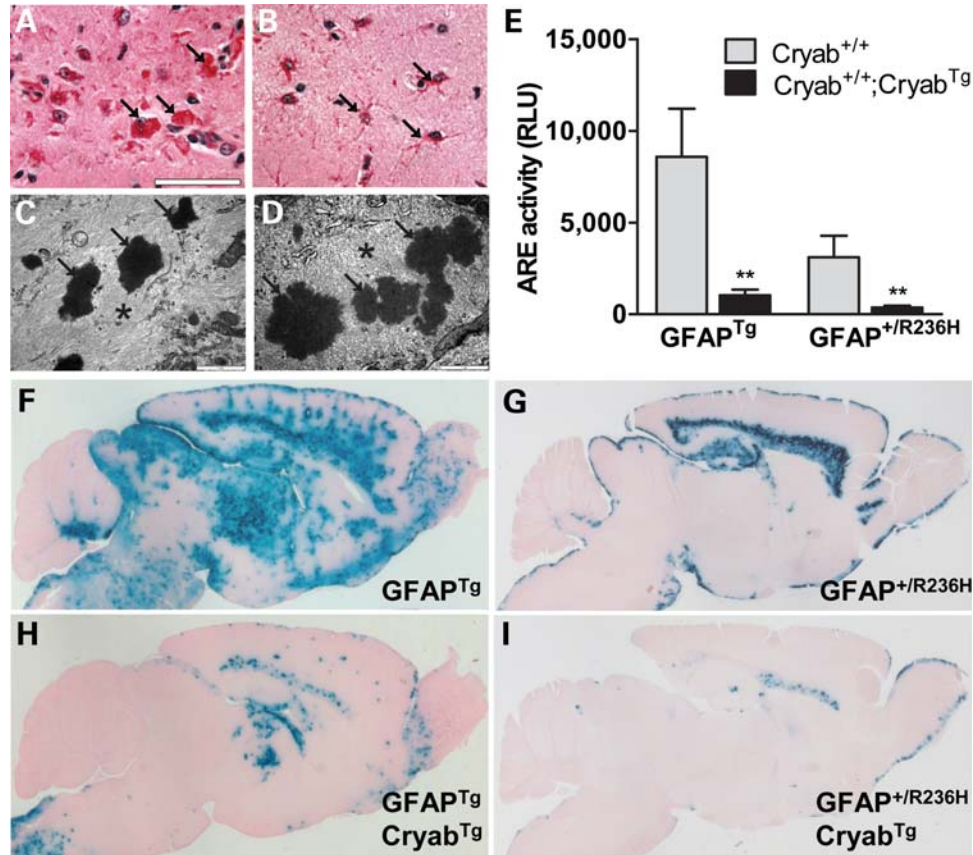


**Figure 5.** Increased expression of Cryab in transgenic mice alters Rosenthal fiber distribution and decreases CNS stress response. (A, B) Rosenthal fiber morphology and cellular distribution in the hippocampus differ between GFAP<sup>Tg</sup> and GFAP<sup>Tg</sup>;Cryab<sup>Tg</sup> mice at 6 weeks, with eosinophilic fibers (arrows) appearing condensed and globular in the GFAP<sup>Tg</sup> mice (A; 50  $\mu$ m scale bar) and punctate or granular and aligned with astrocytic processes in GFAP<sup>Tg</sup>;Cryab<sup>Tg</sup> astrocytes (B). (C, D) Ultrastructural analysis shows Rosenthal fibers as the same dense osmiophilic structures (arrows) among swirls of intermediate filaments (asterisks) regardless of appearance under light microscopy (C, GFAP<sup>Tg</sup>; D, GFAP<sup>Tg</sup>;Cryab<sup>Tg</sup>; 1  $\mu$ m scale bar). (E–I) Elevation of Cryab leads to a decreased stress response in both GFAP<sup>Tg</sup> and GFAP<sup>+R236H</sup> mice. (E) Quantification of alkaline phosphatase reporter activity in whole brain indicates a marked decrease in the ARE response for both GFAP<sup>Tg</sup> (\*\* $P = 0.0012$ ) and GFAP<sup>+R236H</sup> (\*\* $P = 0.0037$ ) mice when positive for Cryab<sup>Tg</sup> (unpaired  $t$ -test, two tailed). RLU, relative luminescence unit; error bars represent standard deviation. (F, G) Histochemistry for ARE-hPAP reporter activity (blue reaction product) indicates a stress response in several regions of the brain for GFAP<sup>Tg</sup> (F) and GFAP<sup>+R236H</sup> (G) mice. This response is greatly diminished in GFAP<sup>Tg</sup>;Cryab<sup>Tg</sup> (H) and GFAP<sup>+R236H</sup>;Cryab<sup>Tg</sup> mice (I) and absent altogether in some regions (6 weeks of age shown).

under normal conditions and is up-regulated in response to diverse types of stress. Several inclusion body disorders of the central nervous system, involving both neurons and glia [including Parkinson's and Alzheimer's diseases, amyotrophic lateral sclerosis (ALS) and AxD], are associated with dramatic increases in the expression of Cryab, often with the crystallin protein accumulating within the inclusions themselves (5,6,34–36). Whether Cryab is a critical determinant of cellular response to injury, and whether its expression could be manipulated for therapeutic benefit in any of these diseases, is not yet known. Large molecular chaperones such as Hsp70 are often elevated in protein misfolding disorders, and expression levels affect aggregate toxicity (34,37), but Hsp70 is not induced, nor is it a component of Rosenthal fibers in AxD models (6,10). Our results suggest that for mouse models of the GFAP-mediated disorder, AxD,  $\alpha$ B-crystallin plays an important role in determining disease severity.

Loss of Cryab alone does not cause an obvious neurological phenotype (38), but recent studies show that Cryab null mice

are more susceptible to EAE, and that astrocytes cultured from these animals show increased cell death and have elevated MAP kinase and NF- $\kappa$ B activation in response to TNF (30). In contrast, a protective effect of enhanced Cryab expression has previously been studied in the heart, where reduction in oxidative stress protected cardiomyocytes from ischemia reperfusion injury (39).

In our AxD model that over-expresses wild-type GFAP, absence of Cryab leads to increased mortality, but our knock-in models that express a disease-associated mutation in GFAP do not show the same effect. Although both lines of mice have elevations in total GFAP, the levels in the wild-type over-expressers are much higher, which may place them at higher risk. Clearly, the stress response as measured by the ARE-reporter is higher and more widely distributed in the GFAP<sup>Tg</sup> mice. It should be noted that the deletion engineered to create the Cryab<sup>-/-</sup> knockout mice also affected the adjacent *Hspb2* gene (38), and it is formally possible that some of the mortality we observe reflects loss of Hspb2 rather than Cryab. However, Hspb2 expression is not normally detected

in brain (40,41), and it is not inducible under the same conditions that induce  $\alpha$ B-crystallin (42). In addition, the ability of GFAP-driven expression of  $\alpha$ B-crystallin to rescue the GFAP<sup>Tg</sup>;Cryab<sup>-/-</sup> animals from death demonstrates that it is the loss of Cryab, and not Hspb2, that is most critical.

Both GFAP<sup>Tg</sup> and GFAP<sup>+R236H</sup> mice demonstrate a marked secondary stress response as evidenced by increased expression of the transcription factor Nrf2 and several stress-responsive genes regulated by Nrf2 through the ARE, including Nqo1 and other genes involved in moderating oxidative toxicity (11,12). Here, we show that increased expression of Cryab dramatically reduces this stress response in both the GFAP transgenic and mutant animals as well as in the combination GFAP<sup>Tg</sup>; GFAP<sup>+R236H</sup> mice. As a chaperone, Cryab may alleviate stress by stabilizing GFAP and the cytoskeleton (20,22) or by promoting proteasomal degradation of corrupt proteins (28,29,43). While elevating Cryab either disaggregates or prevents accumulation of insoluble protein in mice over-expressing wild-type GFAP, it may also chaperone protofilament and tetramer assembly in the soluble pool of GFAP, preventing toxic oligomeric forms (G. Tang, M.D. Perng, R. Friedman, S. Wilk, R. Quinlan, J.E. Goldman, in preparation), similar to those found in other proteinopathies (44). Alternatively, Cryab has also been shown to block activation of RAS (26), which could disrupt downstream activation of MAP kinase signaling pathways and consequently activation of Nrf2 (45).

In the most severe of the animal models examined (the combination GFAP<sup>Tg</sup>; GFAP<sup>+R236H</sup> mice), elevated expression of Cryab in astrocytes restored the expression of Glt1 and prevented terminal seizures. Glutamate transporter expression is altered in several models of neurological disease including ALS, Alzheimer's, Parkinson's and Huntington's disease, as well as epilepsy, stroke and ischemia (33). Glt1 transcription is directly affected by cellular stress through NF- $\kappa$ B and N-myc binding sites in the transporter gene promoter (46), and activation of MAP kinase pathways via the stress response may be responsible for transcriptional repression of Glt1 in our model as well. In addition, Glt1 expression is positively regulated by Akt (47), and we have recently shown a reduction of phosphorylated Akt in cells expressing mutant GFAP (48).

Changes in Cryab and Glt1 expression are common to many of the proteinopathies and may correlate with astrocyte dysfunction and/or gliosis. Huntington's, Parkinson's, spinocerebellar ataxia and ALS all demonstrate non-cell-autonomous pathology in which glial expression of mutant proteins has a toxic effect on vulnerable neurons (49). Although endogenous Cryab is elevated in AxD (36), astrocyte-specific pathology causes severe neurodegeneration with the loss of cortical white matter eventually leading to death, clearly demonstrating a failed protective response. The rescue effect of over-expressing Cryab to suppress cellular stress and maintain astrocyte functions such as glutamate uptake may have wide-ranging implications in the pathogenesis of protein aggregation disorders, and astroprotection should be investigated as therapeutic strategy not only for AxD but also for other degenerative disorders with glial involvement. With the overall reduction in stress response, proteinopathies outside of the CNS, including familial myopathies and hepa-

topathies, where Cryab also accumulates, may benefit from a similar approach.

## MATERIALS AND METHODS

### Transgene construction

To generate an astrocyte-specific  $\alpha$ B-crystallin transgene, the human *GFAP* promoter (50) (position -2163 to +47) was positioned in front of a 6 kb genomic fragment of the hamster  $\alpha$ B-crystallin gene (*Cryab*) (51). The transgene includes the translation initiation site with 90 bp of 5'-UTR, polyadenylation signal and all three exons of *Cryab*. Restriction sites within the cloning plasmid linker sequences were used to ligate the *GFAP* and *Cryab* fragments together. *NotI* was used to excise the transgene (Tg141) from the construct vector (Fig. 2A).

### Mice

$\alpha$ B-crystallin transgenic mice were generated by injecting Tg141 into the pronucleus of fertilized FVB/N ova. Founder lines were maintained in the FVB/N background as hemizygotes. GFAP Tg73.7 transgenic (10) and ARE-hPAP reporter mice (52) were generated as described previously and are also bred in the FVB/N background. Cryab<sup>-/-</sup> knockout mice (38) are maintained as homozygotes in 129S6, and GFAP<sup>+R236H</sup> knock-in mice (12) as heterozygotes in 129S6.

### Western analysis

For Cryab expression in Tg141 mice, protein was extracted from the brain by homogenization in 1% Triton-X-100/1% deoxycholate/0.1% SDS in PBS with 100  $\mu$ g/ml PMSF and Complete Protease Inhibitor Cocktail (Roche Applied Sciences, Indianapolis, IN, USA). After centrifugation at 17 000g for 20 min at 4°C, supernatants were isolated and protein concentrations determined using the BioRad Protein Assay (BioRad, Hercules, CA, USA). For western analysis, extracts from three individual mice (6 weeks of age) for each line were pooled separately to load 50  $\mu$ g/lane on a 10–20% gradient Tris-HCl gel and transferred onto PVDF membrane (BioRad). After blocking in 3% milk/2% normal goat serum in TBS, membranes were probed with polyclonal anti-Cryab (Chemicon AB1546; Millipore, Billerica, MA, USA) and monoclonal anti- $\beta$ -actin (Sigma A-5441; Sigma-Aldrich, St Louis, MO, USA) primary antibodies diluted 1:5000 each in TBS with 0.05% Tween-20 for 16 h at 4°C. After washing with TBS/Tween-20, blots were incubated with peroxidase-conjugated anti-rabbit and mouse IgG, developed with ECL plus, and finally scanned with a Molecular Dynamics Storm phosphorimager (Amersham Biosciences, GE Healthcare, Buckinghamshire, UK). Similar results were observed when protein samples from individual animals were loaded separately.

For Glt1 expression, hippocampal tissues from three animals of each genotype at P25 were homogenized in 2% SDS; 20 mM Tris-HCl, pH 7.4; 2 mM EDTA; 1 mM PMSF with Complete Protease Inhibitor Cocktail (~10  $\mu$ l/mg tissue). Protein concentrations were determined with the

BCA Protein Assay (Pierce Biotechnology, Thermo-Scientific, Rockford, IL, USA), and 12  $\mu\text{g}$  loaded on a 7.5% Tris-HCl polyacrylamide gel and transferred onto PVDF membrane. Blots were treated as described earlier, except probed with polyclonal anti-Glt1 (1:5000, kind gift from Jeffrey Rothstein, Johns Hopkins University School of Medicine, Baltimore, MD, USA) and monoclonal anti-GAPDH (1:2000, Fitzgerald Industries International 10R-G109A, Concord, MA, USA).

### Quantitation of GFAP protein

For GFAP ELISA, hippocampal tissues were homogenized in 10  $\mu\text{l}/\text{mg}$  of 0.5% Triton-X-100; 20 mM Tris-HCl, pH 7.4; 2 mM EDTA; 1 mM PMSF supplemented with Complete Protease Inhibitor Cocktail and centrifuged at 17 000g for 20 min at 4°C. Supernatants were collected as the soluble fraction, and the remaining pellet, representing the insoluble fraction, disrupted in an equivalent volume of 2% SDS and boiled for 15 min (12,43). Protein concentrations of both fractions were quantified separately with the BCA Protein Assay. ELISA was performed in microtiter plates coated with monoclonal anti-GFAP cocktail SMI-26 (1:1000 in PBS; Covance, Princeton, NJ, USA) and blocked with BLOTTO (5% milk in PBS). Protein samples were diluted in PBS with 0.5% Triton-X-100/1% BSA, and 25–500 ng soluble or 5–200 ng insoluble protein analyzed per well. Serial dilutions of purified GFAP (Research Diagnostics, Inc., Flanders, NJ, USA) were used as standards. Polyclonal anti-GFAP was used for the detection antibody (DAKO Z334, Carpinteria, CA, USA) at 200 ng/ml in BLOTTO-TX (0.5% Triton-X-100). Peroxidase-conjugated anti-rabbit IgG antibody (Sigma A6154) was used for the secondary antibody (1:30 000 in BLOTTO-TX). Wells were rinsed with PBS (before the addition of protein samples) or PBS/0.5% Triton-X-100 (after incubation with protein samples) between all incubations. The presence of peroxidase activity was detected with the addition of SuperSignal ELISA Femto Maximum Sensitivity Substrate (Pierce Biotechnology) and quantified with a GloRunner Microplate Luminometer (Turner Biosystems, Sunnyvale, CA, USA).

### Electron microscopy of Rosenthal fibers

Animals were anesthetized and perfused with 10 ml of 0.1 M sodium phosphate buffer, pH 7.4, followed by 50 ml 2.5% glutaraldehyde/2% paraformaldehyde. Brains were removed and post-fixed for 2 h before embedding in Polybed 812. Sections were viewed in a Philips CM120 scanning transmission electron microscope at the University of Wisconsin Medical School Electron Microscopy Facility.

### Immunohistochemistry and immunofluorescence

For ubiquitin immunohistochemistry, animals were anesthetized and perfused with 20 ml PBS, brains removed and immersion-fixed in methacarn overnight, paraffin-embedded and sectioned for slides (6  $\mu\text{m}$ ). Tissue sections were deparaffinized, rehydrated and pre-treated with 0.15%  $\text{H}_2\text{O}_2$  for 10 min, followed by 2 h of blocking in PBS with 10% normal goat serum, 1% BSA and 0.25% Triton-X-100. Sections were incubated with polyclonal anti-ubiquitin

(Novacastra, NCL-UBIQ; Vector Laboratories, Burlingame, CA, USA) diluted 1:500 in block overnight at 4°C, followed by biotinylated goat anti-rabbit IgG (1:200) for 2 h, avidin/biotin-peroxidase complex solution for 30 min (Elite ABC Kit, Vector Laboratories), followed by Vector SG substrate for 10 min. Tissues were rinsed thoroughly with PBS between all incubations.

For Cryab, GFAP and NeuN immunofluorescence, animals were perfused with Histochoice MB fixative with 20% ethanol (Amresco, Solon, OH, USA), brains removed and post-fixed overnight, dehydrated and embedded in paraffin for sectioning. Tissue sections were treated as described previously without  $\text{H}_2\text{O}_2$  pre-treatment and incubated with monoclonal anti-GFAP (1:500; Chemicon MAB3402), monoclonal anti-NeuN (1:400; Chemicon MAB377) and/or polyclonal anti-Cryab (1:200; antibody 3148, kind gift from Roy Quinlan, University of Durham, Durham, UK) (53) at 4°C for  $\sim 16$  h, followed by incubation with secondary antibodies Alexafluor-594-conjugated goat anti-mouse IgG<sub>1</sub> (1:200, Molecular Probes, Eugene, OR, USA) and FITC-conjugated goat anti-rabbit IgG (1:100, Sigma F0382). Images were taken with a Nikon C1 laser scanning confocal microscope.

### ARE-hPAP histochemistry and quantitative assay

For alkaline phosphatase histochemistry, animals were perfused with 10 ml PBS, followed by 50 ml 4% paraformaldehyde. Brains were immersion-fixed for 2 h, alcohol-dehydrated, paraffin-embedded and sectioned for slides (6  $\mu\text{m}$ ). After de-paraffinizing and rehydration, sections were heated at 65°C for 45 min in AP buffer (0.1 M Tris, pH 9.5/0.1 M NaCl/5 mM  $\text{MgCl}_2$ ) to inactivate endogenous alkaline phosphatases. Sections were then incubated in AP buffer with 0.17 mg/ml 5-bromo-4-chloro-3-indolyl phosphate (Sigma B6149) for 48 h at 37°C. Sections were rinsed, counterstained with eosin, dehydrated and coverslips applied.

To quantitate and compare the level of reporter gene activity, half-brain samples (bisected at midline) were homogenized in 1 ml lysate buffer (50 mM Tris-HCl, pH 7.5/5 mM  $\text{MgCl}_2$ /100 mM NaCl/4% CHAPS) and centrifuged at 17 000g for 20 min at 4°C. Supernatants were collected and protein quantified with the BioRad Protein Assay (Hercules, CA, USA). Samples were diluted to 100 ng/ $\mu\text{l}$ , 25  $\mu\text{l}$  added to 75  $\mu\text{l}$  200 mM diethanolamine (DEA) in a microtiter plate and heated for 20 min at 65°C to inactivate endogenous alkaline phosphatase activity. At room temperature, 100  $\mu\text{l}$  chemiluminescent substrate CSPD with Emerald enhancer (2 $\times$ ; Tropix-Applied Biosystems, Bedford, MA, USA) in 5 mM  $\text{MgCl}_2$ /150 mM DEA was added to each well, incubated at room temperature for 20 min, and enzyme activity measured with a GloRunner Microplate Luminometer.

### Quantitative PCR for stress response transcripts and glutamate transporters

Real-time PCR was performed with samples from four mice at P26 for each genotype in the 129SFVBF1 hybrid background. Quantitative PCR was performed as described previously (11). Transcript-specific sequences (Supplementary Material, Table S2) were amplified from hippocampus cDNA in a

reaction with SYBR Green PCR Master Mix (Applied Biosystems, Foster City, CA, USA) and quantitated with an Applied Biosystems 7500 Real-Time PCR System.

### Statistics

For direct comparisons of transcript and protein levels between relevant genotypes, unpaired two-tailed *t*-tests were used to generate *P*-values; for survival curves, log-rank Mantel–Cox analysis. All analyses were performed using GraphPad Prism Software, version 5.01 (San Diego, California, CA, USA).

### SUPPLEMENTARY MATERIAL

Supplementary Material is available at *HMG* online.

### ACKNOWLEDGEMENTS

We sincerely thank Heide Peickert, Charanjeet Kaur, Allison Goff and Denice Springman for technical support; Benjamin August for electron microscopy; and Michael Brenner, James E. Goldman, Roy Quinlan and Maiken Nedergaard for critical review and suggestions on this manuscript.

*Conflict of Interest statement.* None declared.

### FUNDING

This work was supported by National Institutes of Health Grants NS060120, NS42803 and HD03352.

### REFERENCES

- Alexander, W.S. (1949) Progressive fibrinoid degeneration of fibrillary astrocytes associated with mental retardation in a hydrocephalic infant. *Brain*, **72**, 373–381.
- Brenner, M., Johnson, A.B., Boespflug-Tanguy, O., Rodriguez, D., Goldman, J.E. and Messing, A. (2001) Mutations in GFAP, encoding glial fibrillary acidic protein, are associated with Alexander disease. *Nat. Genet.*, **27**, 117–120.
- Li, R., Johnson, A.B., Salomons, G., Goldman, J.E., Naidu, S., Quinlan, R., Cree, B., Ruyle, S.Z., Banwell, B., D'Hooghe, M. *et al.* (2005) Glial fibrillary acidic protein mutations in infantile, juvenile, and adult forms of Alexander disease. *Ann. Neurol.*, **57**, 310–326.
- Tian, R., Gregor, M., Wiche, G. and Goldman, J.E. (2006) Plectin regulates the organization of glial fibrillary acidic protein in Alexander disease. *Am. J. Pathol.*, **168**, 888–897.
- Iwaki, T., Iwaki, A., Tateishi, J., Sakaki, Y. and Goldman, J.E. (1993) Alpha B-crystallin and 27-kd heat shock protein are regulated by stress conditions in the central nervous system and accumulate in Rosenthal fibers. *Am. J. Pathol.*, **143**, 487–495.
- Der Perng, M., Su, M., Wen, S.F., Li, R., Gibbon, T., Prescott, A.R., Brenner, M. and Quinlan, R.A. (2006) The Alexander disease-causing glial fibrillary acidic protein mutant, R416W, accumulates into Rosenthal fibers by a pathway that involves filament aggregation and the association of alpha B-crystallin and HSP27. *Am. J. Hum. Genet.*, **79**, 197–213.
- Ross, C.A. and Poirier, M.A. (2005) Opinion: what is the role of protein aggregation in neurodegeneration? *Nat. Rev. Mol. Cell Biol.*, **6**, 891–898.
- Brenner, M., Goldman, J.E., Quinlan, R.A. and Messing, A. (2008) Alexander disease: a genetic disorder of astrocytes. In Pappas, V. and Haydon, P.G. (eds). *Astrocytes in Pathophysiology of the Nervous System*. Springer, pp. 591–648.
- Mignot, C., Boespflug-Tanguy, O., Gelot, A., Dautigny, A., Pham-Dinh, D. and Rodriguez, D. (2004) Alexander disease: putative mechanisms of an astrocytic encephalopathy. *Cell Mol. Life Sci.*, **61**, 369–385.
- Messing, A., Head, M.W., Galles, K., Galbreath, E.J., Goldman, J.E. and Brenner, M. (1998) Fatal encephalopathy with astrocyte inclusions in GFAP transgenic mice. *Am. J. Pathol.*, **152**, 391–398.
- Hagemann, T.L., Gaeta, S.A., Smith, M.A., Johnson, D.A., Johnson, J.A. and Messing, A. (2005) Gene expression analysis in mice with elevated glial fibrillary acidic protein and Rosenthal fibers reveals a stress response followed by glial activation and neuronal dysfunction. *Hum. Mol. Genet.*, **14**, 2443–2458.
- Hagemann, T.L., Connor, J.X. and Messing, A. (2006) Alexander disease-associated glial fibrillary acidic protein mutations in mice induce Rosenthal fiber formation and a white matter stress response. *J. Neurosci.*, **26**, 11162–11173.
- Hsiao, V.C., Tian, R., Long, H., Der Perng, M., Brenner, M., Quinlan, R.A. and Goldman, J.E. (2005) Alexander-disease mutation of GFAP causes filament disorganization and decreased solubility of GFAP. *J. Cell Sci.*, **118**, 2057–2065.
- Kappe, G., Franck, E., Verschuere, P., Boelens, W.C., Leunissen, J.A. and de Jong, W.W. (2003) The human genome encodes 10 alpha-crystallin-related small heat shock proteins: HspB1–10. *Cell Stress Chaperones*, **8**, 53–61.
- Klemenz, R., Fröhli, E., Steiger, R.H., Schäfer, R. and Aoyama, A. (1991) Alpha B-crystallin is a small heat shock protein. *Proc. Natl Acad. Sci. USA*, **88**, 3652–3656.
- Horwitz, J. (1992) Alpha-crystallin can function as a molecular chaperone. *Proc. Natl Acad. Sci. USA*, **89**, 10449–10453.
- Jakob, U., Gaestel, M., Engel, K. and Buchner, J. (1993) Small heat shock proteins are molecular chaperones. *J. Biol. Chem.*, **268**, 1517–1520.
- Kato, K., Shinohara, H., Kurobe, N., Inaguma, Y., Shimizu, K. and Ohshima, K. (1991) Tissue distribution and developmental profiles of immunoreactive alpha B crystallin in the rat determined with a sensitive immunoassay system. *Biochim. Biophys. Acta*, **1074**, 201–208.
- Klemenz, R., Andres, A.C., Frohli, E., Schafer, R. and Aoyama, A. (1993) Expression of the murine small heat shock proteins hsp 25 and alpha B crystallin in the absence of stress. *J. Cell Biol.*, **120**, 639–645.
- Perng, M.D., Cairns, L., van den IJssel, P., Prescott, A., Hutcheson, A.M. and Quinlan, R.A. (1999) Intermediate filament interactions can be altered by HSP27 and alphaB-crystallin. *J. Cell Sci.*, **112**, 2099–2112.
- Bennardini, F., Wrzosek, A. and Chiesi, M. (1992) Alpha B-crystallin in cardiac tissue. Association with actin and desmin filaments. *Circ. Res.*, **71**, 288–294.
- Nicholl, I.D. and Quinlan, R.A. (1994) Chaperone activity of alpha-crystallins modulates intermediate filament assembly. *EMBO J.*, **13**, 945–953.
- Ghosh, J.G., Houck, S.A. and Clark, J.I. (2007) Interactive sequences in the stress protein and molecular chaperone human alphaB crystallin recognize and modulate the assembly of filaments. *Int. J. Biochem. Cell Biol.*, **39**, 1804–1815.
- Kamradt, M.C., Chen, F. and Cryns, V.L. (2001) The small heat shock protein alpha B-crystallin negatively regulates cytochrome c- and caspase-8-dependent activation of caspase-3 by inhibiting its autoproteolytic maturation. *J. Biol. Chem.*, **276**, 16059–16063.
- Mao, Y.W., Liu, J.P., Xiang, H. and Li, D.W. (2004) Human alphaA- and alphaB-crystallins bind to Bax and Bcl-X(S) to sequester their translocation during staurosporine-induced apoptosis. *Cell Death Differ.*, **11**, 512–526.
- Li, D.W., Liu, J.P., Mao, Y.W., Xiang, H., Wang, J., Ma, W.Y., Dong, Z., Pike, H.M., Brown, R.E. and Reed, J.C. (2005) Calcium-activated RAF/MEK/ERK signaling pathway mediates p53-dependent apoptosis and is abrogated by alpha B-crystallin through inhibition of RAS activation. *Mol. Biol. Cell.*, **16**, 4437–4453.
- Mehlen, P., Kretz-Remy, C., Preville, X. and Arrigo, A.P. (1996) Human hsp27, *Drosophila* hsp27 and human alphaB-crystallin expression-mediated increase in glutathione is essential for the protective activity of these proteins against TNFalpha-induced cell death. *EMBO J.*, **15**, 2695–2706.
- Boelens, W.C., Croes, Y. and de Jong, W.W. (2001) Interaction between alphaB-crystallin and the human 20S proteasomal subunit C8/alpha7. *Biochim. Biophys. Acta*, **1544**, 311–319.

29. den Engelsman, J., Keijsers, V., de Jong, W.W. and Boelens, W.C. (2003) The small heat-shock protein alpha B-crystallin promotes FBX4-dependent ubiquitination. *J. Biol. Chem.*, **278**, 4699–4704.
30. Ousman, S.S., Tomooka, B.H., van Noort, J.M., Wawrousek, E.F., O'Connor, K.C., Hafler, D.A., Sobel, R.A., Robinson, W.H. and Steinman, L. (2007) Protective and therapeutic role for alphaB-crystallin in autoimmune demyelination. *Nature*, **448**, 474–479.
31. Koyama, Y. and Goldman, J.E. (1999) Formation of GFAP cytoplasmic inclusions in astrocytes and their disaggregation by alphaB-crystallin. *Am. J. Pathol.*, **154**, 1563–1572.
32. Herndon, R.M., Rubinstein, L.J., Freeman, J.M. and Mathieson, G. (1970) Light and electron microscopic observations on Rosenthal fibers in Alexander's disease and in multiple sclerosis. *J. Neuropathol. Exp. Neurol.*, **29**, 524–551.
33. Maragakis, N.J. and Rothstein, J.D. (2004) Glutamate transporters: animal models to neurologic disease. *Neurobiol. Dis.*, **15**, 461–473.
34. Muchowski, P.J. and Wacker, J.L. (2005) Modulation of neurodegeneration by molecular chaperones. *Nat. Rev. Neurosci.*, **6**, 11–22.
35. Arrigo, A.P., Simon, S., Gibert, B., Kretz-Remy, C., Nivon, M., Czekalla, A., Guillet, D., Moulin, M., Diaz-Latoud, C. and Vicart, P. (2007) Hsp27 (HspB1) and alphaB-crystallin (HspB5) as therapeutic targets. *FEBS Lett.*, **581**, 3665–3674.
36. Iwaki, T., Kume-Iwaki, A., Liem, R.K. and Goldman, J.E. (1989) Alpha B-crystallin is expressed in non-lenticular tissues and accumulates in Alexander's disease brain. *Cell*, **57**, 71–78.
37. Auluck, P.K., Chan, H.Y., Trojanowski, J.Q., Lee, V.M. and Bonini, N.M. (2002) Chaperone suppression of alpha-synuclein toxicity in a *Drosophila* model for Parkinson's disease. *Science*, **295**, 865–868.
38. Brady, J.P., Garland, D.L., Green, D.E., Tamm, E.R., Giblin, F.J. and Wawrousek, E.F. (2001) AlphaB-crystallin in lens development and muscle integrity: a gene knockout approach. *Invest. Ophthalmol. Vis. Sci.*, **42**, 2924–2934.
39. Ray, P.S., Martin, J.L., Swanson, E.A., Otani, H., Dillmann, W.H. and Das, D.K. (2001) Transgene overexpression of alphaB crystallin confers simultaneous protection against cardiomyocyte apoptosis and necrosis during myocardial ischemia and reperfusion. *FASEB J.*, **15**, 393–402.
40. Iwaki, A., Nagano, T., Nakagawa, M., Iwaki, T. and Fukumaki, Y. (1997) Identification and characterization of the gene encoding a new member of the alpha-crystallin/small hsp family, closely linked to the alphaB-crystallin gene in a head-to-head manner. *Genomics*, **45**, 386–394.
41. Quraisha, S., Asuni, A., Boelens, W.C., O'Connor, V. and Wyttenbach, A. (2008) Expression of the small heat shock protein family in the mouse CNS: differential anatomical and biochemical compartmentalization. *Neuroscience*, **153**, 483–491.
42. Suzuki, A., Sugiyama, Y., Hayashi, Y., Nyu-i, N., Yoshida, M., Nonaka, I., Ishiura, S., Arahata, K. and Ohno, S. (1998) MKBP, a novel member of the small heat shock protein family, binds and activates the myotonic dystrophy protein kinase. *J. Cell Biol.*, **140**, 1113–1124.
43. Tang, G., Xu, Z. and Goldman, J.E. (2006) Synergistic effects of the SAPK/JNK and the proteasome pathway on glial fibrillary acidic protein (GFAP) accumulation in Alexander disease. *J. Biol. Chem.*, **281**, 38634–38643.
44. Ross, C.A. and Poirier, M.A. (2004) Protein aggregation and neurodegenerative disease. *Nat. Med.*, **10** (suppl.), S10–S17.
45. McCubrey, J.A., Lahair, M.M. and Franklin, R.A. (2006) Reactive oxygen species-induced activation of the MAP kinase signaling pathways. *Antioxid. Redox Signal.*, **8**, 1775–1789.
46. Sitcheran, R., Gupta, P., Fisher, P.B. and Baldwin, A.S. (2005) Positive and negative regulation of EAAT2 by NF-kappaB: a role for N-myc in TNFalpha-controlled repression. *EMBO J.*, **24**, 510–520.
47. Li, L.B., Toan, S.V., Zelenia, O., Watson, D.J., Wolfe, J.H., Rothstein, J.D. and Robinson, M.B. (2006) Regulation of astrocytic glutamate transporter expression by Akt: evidence for a selective transcriptional effect on the GLT-1/EAAT2 subtype. *J. Neurochem.*, **97**, 759–771.
48. Tang, G., Yue, Z., Talloczy, Z., Hagemann, T., Cho, W., Messing, A., Sulzer, D.L. and Goldman, J.E. (2008) Autophagy induced by Alexander disease-mutant GFAP accumulation is regulated by p38/MAPK and mTOR signaling pathways. *Hum. Mol. Genet.*, **17**, 1540–1555.
49. Lobsiger, C.S. and Cleveland, D.W. (2007) Glial cells as intrinsic components of non-cell-autonomous neurodegenerative disease. *Nat. Neurosci.*, **10**, 1355–1360.
50. Brenner, M., Kisseberth, W.C., Su, Y., Besnard, F. and Messing, A. (1994) GFAP promoter directs astrocyte-specific expression in transgenic mice. *J. Neurosci.*, **14**, 1030–1037.
51. Quax-Jeuken, Y., Quax, W., van Rens, G., Khan, P.M. and Bloemendal, H. (1985) Complete structure of the alpha B-crystallin gene: conservation of the exon–intron distribution in the two nonlinked alpha-crystallin genes. *Proc. Natl Acad. Sci. USA*, **82**, 5819–5823.
52. Johnson, D.A., Andrews, G.K., Xu, W. and Johnson, J.A. (2002) Activation of the antioxidant response element in primary cortical neuronal cultures derived from transgenic reporter mice. *J. Neurochem.*, **81**, 1233–1241.
53. van den IJssel, P., Wheelock, R., Prescott, A., Russell, P. and Quinlan, R.A. (2003) Nuclear speckle localisation of the small heat shock protein alpha B-crystallin and its inhibition by the R120G cardiomyopathy-linked mutation. *Exp. Cell Res.*, **287**, 249–261.